UNIVERSITY OF CAMBRIDGE

Numerical Analysis Reports

Split-Hamiltonian Methods for Rigid Body Molecular Dynamics

A. Dullweber
B. Leimkuhler
R. McLachlan

DAMTP 1997/NA11
May 1997

Department of Applied Mathematics and Theoretical Physics
Silver Street
Cambridge
England CB3 9EW

Split-Hamiltonian Methods for Rigid Body Molecular Dynamics

Andreas Dullweber

University Chemical Laboratories, Lensfield Road, Cambridge CB2 1EW, UK

Benedict Leimkuhler†

Department of Mathematics, the University of Kansas, Lawrence, KS 66045, U.S.A.

Robert McLachlan‡

Department of Mathematics, Massey University, Palmerston North, New Zealand

Abstract

Rigid body molecular models possess symplectic structure and time-reversal symmetry. Standard numerical integration methods destroy both properties, introducing nonphysical dynamical behavior such as numerically-induced dissipative states and drift in the energy during long term simulations. This article describes the construction, implementation and practical application of fast explicit symplectic-reversible integrators for multiple rigid body molecular simulations. These methods use a reduction to Euler equations for the free rigid body, together with a symplectic Hamiltonian splitting technique. In every timestep, the orientational dynamics of each rigid body are integrated by a sequence of planar rotations. Besides preserving the symplectic and reversible structures of the flow, this scheme accurately conserves the total angular momentum of a system of interacting rigid bodies. Excellent energy conservation can be obtained relative to traditional methods, especially in long time simulations. The method is implemented in a research code, ORIENT, and compared with a quaternion/extrapolation scheme for the TIP4P model of water. Our experiments show that the symplectic-reversible is far superior to the more traditional quaternion method.

keywords: Rigid body simulations, molecular dynamics, symplectic discretizations, site to site and dipolar potentials, TIP4P water.

---

†Visiting Department of Applied Mathematics and Theoretical Physics, Cambridge, UK, 1996-97. Research supported by NSF 9303223 and DAMTP.

‡Visitor at the Isaac Newton Institute for Mathematical Sciences, Cambridge, UK, 1996

I. INTRODUCTION

Rigid body molecular dynamics simulations are an increasingly important tool in chemical and physical research.[1,2] With steady increases in the size of systems under study and the time intervals over which simulations are carried out, and to keep pace with improvements in the realism of molecular models, better numerical integration schemes are also needed. Symplectic and time-reversible integration methods are schemes which automatically preserve a corresponding mechanical structure of the phase flow. While the primary motivation for mathematical study of geometric integrators—as opposed to more traditional numerical schemes—may be largely æsthetic, there is growing evidence that, particularly in large or lengthy computations, these geometrical integrators can provide clear-cut efficiency and stability improvements over standard integration schemes.[3–7]

For rigid bodies, the traditional use of parameters to represent the motion (e.g. quaternions) leads to a straightforward integration technique using standard numerical integration methods such as explicit Runge-Kutta methods, predictor-corrector schemes, and Gragg-Bulirsch-Stoer extrapolation.[8,9] However, the parameterized description introduces additional coupling in the Hamiltonian between positions and momenta, and effectively prevents the use of efficient (explicit) integration methods that are symplectic and/or time-reversible. The loss of structure manifests itself in an energy drift during long-time simulations. Correcting this drift by such measures as rescaling of the velocities[9] does not improve stability. In practice, very small steps in time often must be used in order to limit the energy drift. Moreover, the loss of physicality associated to the destruction of structure can manifest itself in peculiar nonphysical behavior: in the next section we show that a discretization of a single rigid body using a nonsymplectic explicit Runge-Kutta discretization may have *asymptotically stable (dissipative) fixed points*, something which is impossible in the true symplectic flow (or under symplectic discretization).

One of the authors recently reported outstanding stability and efficiency improvements using a partially implicit symplectic and reversible method for rigid body molecular dynamics simulations.[7,10] This method employed a canonical rotation matrix formulation for each body and used constrained SHAKE[11] integration to preserve orthogonality. In the current article, we further improve on this idea by using instead an integration method based on the classical mechanics concepts of contstrained dynamics, splitting, and "reduction."[12] Specifically, the Hamiltonian is broken up so that the rotational free-body dynamics are decoupled from the interaction terms. Each free rigid body is then integrated in Euler (momentum) representation using a further splitting into integrable parts. The result is an *explicit* scheme which constructs the numerical solution by concatenation of integrable flows, and thus automatically conserves the symplectic structure. A symmetric decomposition insures time-reversibility, and the method can also be shown to conserve total angular momentum. Our approach is based on a splitting technique for treating a free rigid body independently proposed by Reich[13] and McLachlan[14] which was later extended by Reich[15] into a scheme for simulating a rigid body in a potential field. The current article shows that for realistic molecular applications involving multiple rigid bodies, the explicit symplectic approach is not only competitive but generally far superior to the traditional quaternion-based integration approach.

Compared to standard methods, the symplectic approach is more stable, enabling the use of larger timesteps. Compared to the semi-explicit SHAKE-based scheme,[7,10] the splitting method is more efficient (since it is explicit). For multiple rigid bodies not coupled by constraints, the splitting method thus appears to offer a substantial improvement over existing schemes.

II. SYMPLECTIC METHODS

In this section, we introduce the concept of a symplectic method by deriving the popular Verlet (leapfrog) integrator used in N-body simulations by splitting the Hamiltonian. We then show that a similar type of integrator can be used to develop an integrator for a single rigid body, and we show that the latter approach behaves more reliably than a Runge-Kutta method.

A. Verlet as a Symplectic Splitting Method

For systems with a Hamiltonian of the form $H = T(\boldsymbol{p}) + V(\boldsymbol{q})$, the Verlet method provides a simple approach to symplectic integration.[16] Here

$$T(\boldsymbol{p}) = \frac{1}{2}\boldsymbol{p}^T \boldsymbol{M}^{-1}\boldsymbol{p}$$

is the kinetic energy ($\boldsymbol{M}$ is a mass matrix), and V is the potential energy. The Verlet method can be viewed as constructing an approximate solution by pasting together the exact solutions of the kinetic and potential parts of H.[5,16]

That is, given positions $\boldsymbol{q}^n$ and momenta $\boldsymbol{p}^n$, which approximate the solution at time $t = t_0 + n\Delta t$, we first compute the exact solution to just the potential part of the Hamiltonian for a step of size $\frac{1}{2}\Delta t$ in time. Since the equations of motion for $V = V(\boldsymbol{q})$ are

$$\begin{aligned} &\frac{d}{dt}\boldsymbol{q} = 0, \\ &\frac{d}{dt}\boldsymbol{p} = \boldsymbol{f}(\boldsymbol{q}) \equiv -\nabla_{\boldsymbol{q}} V, \end{aligned}$$

we notice that we can solve them exactly: $\boldsymbol{q}$ is constant during the step ($\boldsymbol{q} \equiv \boldsymbol{q}^n$) and $\boldsymbol{p}$ undergoes a linear motion from $\boldsymbol{p}^n$ to $\boldsymbol{p}^{n+1/2}$:

$$\boldsymbol{p}^{n+1/2} = \boldsymbol{p}^n + \boldsymbol{f}(\boldsymbol{q}^n).$$

We next solve just the kinetic term for one full step in time, during which the momenta are constant (since T is independent of $\boldsymbol{q}$) and the positions evolve in straight line motion:

$$\boldsymbol{q}^{n+1} = \boldsymbol{q}^n + \Delta t \boldsymbol{M}^{-1}\boldsymbol{p}^{n+1/2}.$$

Finally, we update $\boldsymbol{p}$ again by integrating the potential term for one half timestep:

$$\boldsymbol{p}^{n+1} = \boldsymbol{p}^{n+1/2} + \boldsymbol{f}(\boldsymbol{q}^{n+1}).$$

The fact that the numerical solution is constructed by stringing together a sequence of exact solutions of partial Hamiltonians ensures that the result will be a symplectic method. Although symplectic methods can be constructed by other techniques,[3] it is the splitting methods which typically prove to be most useful in applications.[4,6,5] The leapfrog method also respects the time-reversal symmetry of the equations, and it preserves to within a small multiple of computer rounding error the angular momentum of a system of particles (in the absence of periodic boundaries). An extension of the leapfrog method, SHAKE, is available for holonomically constrained N-body simulations and is also symplectic and time-reversible.[17]

Symplectic methods can be shown to exactly conserve a nearby energy function $\widetilde{H} \approx H$. This in turn can be shown to ensure long term approximate conservation of energy in certain cases[18]. That reference also shows that in "scattering" events, such as the close approach of one rigid body to another, integrators like Verlet conserve the local energy and angular momentum essentially exactly. This is a particularly nice feature since it is these events that cause trouble when using standard methods. It is also easy to build extra properties such as conservation of momentum and reversibility into symplectic integrators. They show excellent long term stability and fidelity to the properties of solutions of the continuous model; in some sense they report qualitatively correct dynamics in complex situations which cannot be followed to high accuracy.[3] Finally, since they are simple, fast, and explicit, we consider them excellent for large molecular dynamics simulations.

B. A Single Rigid Body

As an example, we now consider the example of single axially symmetric rigid body spinning in a linear potential field and pinned at one point along its axis of symmetry. The simplest physical interpretation is a heavy "Lagrange top," but we could also suppose it to model a molecular fragment acted on by a charge distant enough to permit linearization of the potential. This simple model illustrates in a striking fashion the advantages of symplectic methods over nonsymplectic schemes, even when the former are of lower classical order of accuracy.

We will assume that the components of the diagonalized inertial tensor in body coordinates are $I_1 = I_2 = 1$, with I_3 treated as a free parameter. We will also assume that the mass, the gravitational constant, and the distance from the center of mass to the fixed point are all one. The equations of motion can be developed in terms of a unit vector $\boldsymbol{u} = (u_1, u_2, u_3)$ representing the orientation of the body relative to a fixed reference configuration, and the angular momenta π_i, $i = 1, 2, 3$, using a generalized Hamiltonian formalism.[12] The u_i can be viewed as playing a similar role to quaternions. The energy of the system is given by:

$$H = H(\boldsymbol{\pi}, \boldsymbol{u}) = \frac{1}{2}(\pi_1^2 + \pi_2^2 + \frac{1}{I_3}\pi_3^2) + u_3,$$

and the equations are Hamiltonian with respect to the Poisson bracket

$$\{F, G\} := -\boldsymbol{\pi} \cdot (\nabla_{\boldsymbol{\pi}} F \times \nabla_{\boldsymbol{\pi}} G) - \boldsymbol{u} \cdot (\nabla_{\boldsymbol{\pi}} F \times \nabla_{\boldsymbol{u}} G - \nabla_{\boldsymbol{\pi}} G \times \nabla_{\boldsymbol{u}} F).$$

This means that each of the components of the vector field is constructed by computing the Poisson bracket of the associated variable with the Hamiltonian function:

$$\frac{d}{dt}u_1 = \{u_1, H\} = \frac{u_2\pi_3}{I_3} - u_3\pi_2,$$

and so on.

We will compare the numerical solution using a popular fourth order Runge-Kutta method[8] with the results obtained from the symplectic splitting method.[13,14]

This approach is derived in a similar way to the leapfrog method. We first split H into four pieces:

$$H = H_1 + H_2 + H_3 + H_4,$$

$$H_1 = \frac{1}{2}\pi_1^2, \quad H_2 = \frac{1}{2}\pi_2^2, \quad H_3 = \frac{1}{2I_3}\pi_3^2, \quad H_4 = u_3$$

Each of these terms is completely integrable. For example, the solution evolves under the first term according to

$$\begin{aligned} \tfrac{d}{dt}u_1 &= 0, & \tfrac{d}{dt}\pi_1 &= 0, \\ \tfrac{d}{dt}u_2 &= \pi_1 u_3, & \tfrac{d}{dt}\pi_2 &= \pi_1\pi_3, \\ \tfrac{d}{dt}u_3 &= -\pi_1 u_2, & \tfrac{d}{dt}\pi_3 &= -\pi_1\pi_2 \end{aligned}$$

Both terms are thus integrated in terms of identical simultaneous planar rotations. Similar equations are obtained for H_2 and H_3, while under H_4, only $\boldsymbol{\pi}$ evolves, and according to

$$\begin{aligned} \frac{d}{dt}\pi_1 &= u_2 \\ \frac{d}{dt}\pi_2 &= -u_1. \end{aligned}$$

which is just straight line motion.

The flow map of H is approximated within a timestep by the concatenation of the flows on each of the four terms. This method is only first order, but it is symplectic.

As a numerical experiment, we solved the top using the popular explicit 4th order Runge-Kutta method. The motion of the center of mass from typical initial conditions is periodic or quasiperiodic. We first chose $I_3 = 1$ (spherical top) and integrated the motion from various initial values. In Fig. 1 we show two trajectories along with the associated variation in energy, for $\Delta t = 0.1$. Note that there is a clear secular (linear) drift in the energy with time. This qualitative behavior is observed regardless of timestep, as long as it is sufficiently small, although the actual magnitude of the energy variation does of course depend on stepsize. Moreover, this type of drift would be expected essentially regardless of the integration strategy used, as long as it is not a symplectic or reversible method.

The results of integrating instead with the symplectic scheme are shown in Fig. 2. The energy fluctuation is greater, but there is no evident drift. The large difference in magnitude of the energy error is the result of the higher order of accuracy of the Runge-Kutta method (we are using the same stepsize of $\Delta t = 0.1$; it could be eliminated by using a higher order symplectic method instead of the simple splitting scheme.

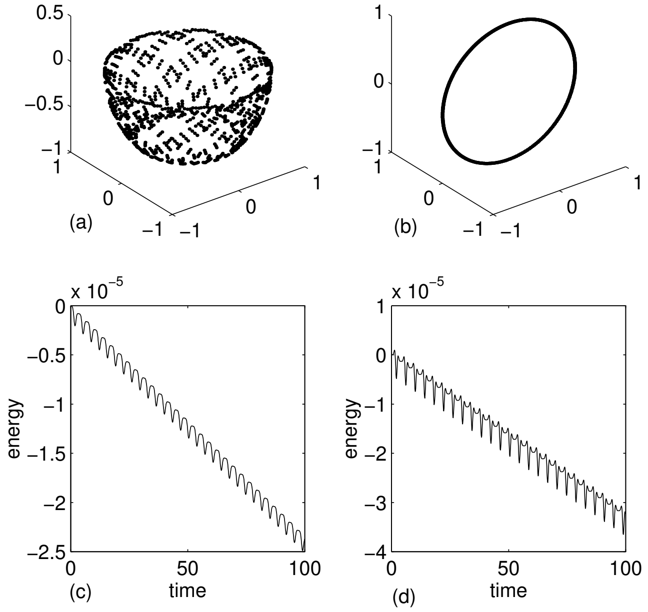

FIG. 1. Integrations performed with the fourth order Runge-Kutta method ($\Delta t = 0.1$): (a) $\boldsymbol{u}$ is plotted at each timestep for a quasiperiodic orbit of the spherical top, started from $\boldsymbol{u}(0) = (0, 1, 0), \boldsymbol{\pi}(0) = (0, 0, -1)$, (b) a periodic solution from $\boldsymbol{u}(0) = (0, 0, 1), \boldsymbol{\pi}(0) = (0, 1, 0)$, (c) energy error for (a), (d) energy error for (b).

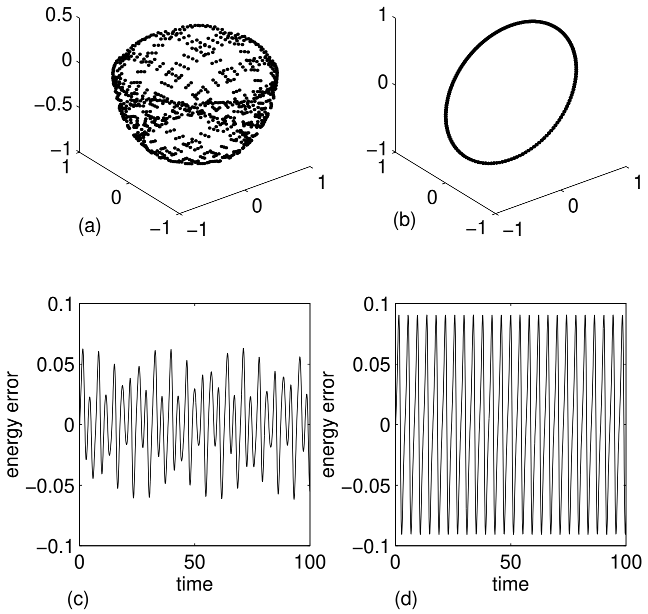

FIG. 2. The top solved using the first order symplectic method ($\Delta t = 0.1$), and initial conditions as in Fig. 1: (a) quasiperiodic solution, (b) periodic solution, (c) energy error for (a), and (d) energy error for (b).

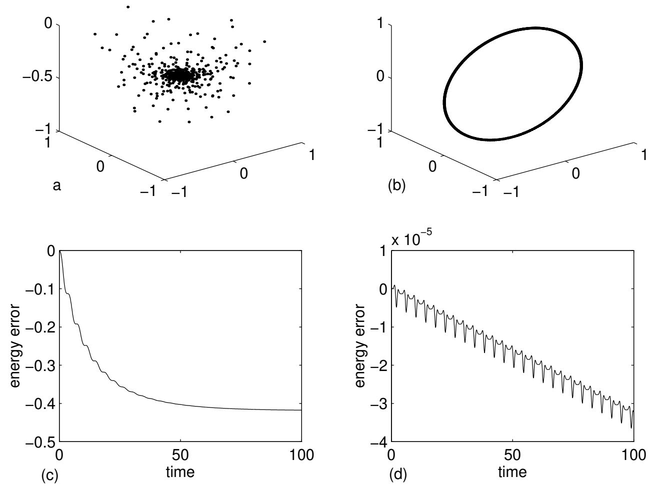

FIG. 3. The Runge-Kutta method ($\Delta t = 0.1$) on the *skinny top*, initial conditions as in Fig. 1: (a) quasiperiodic orbit, the successive points rapidly decay toward the upright position! (b) periodic solution, (c) energy error for (a), (d) energy error for (b).

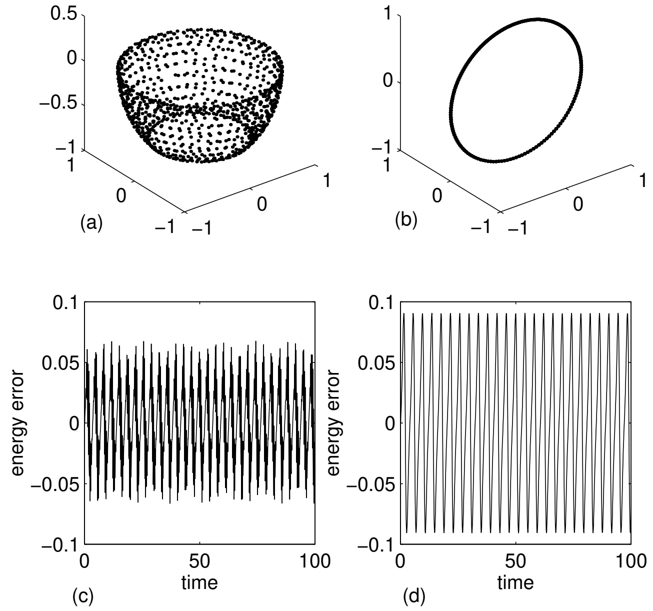

FIG. 4. The symplectic method applied to the skinny top ($\Delta t = 0.1$), initial conditions as in Fig. 1: (a) quasiperiodic solution, (b) periodic solution, (c) energy error for (a), (d) energy error for (b).

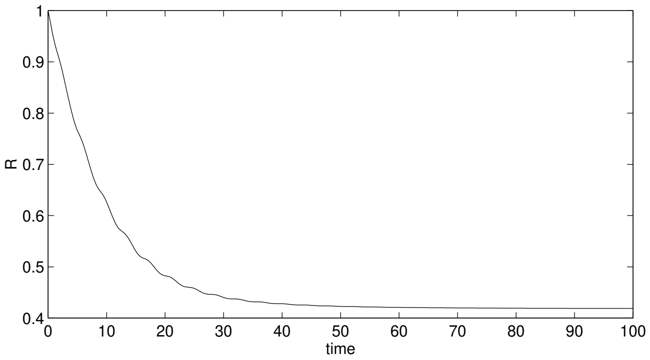

FIG. 5. The length, $R = (u_1^2 + u_2^2 + u_3^2)^{1/2}$, of the unit vector associated to the top along the solution of 3a.

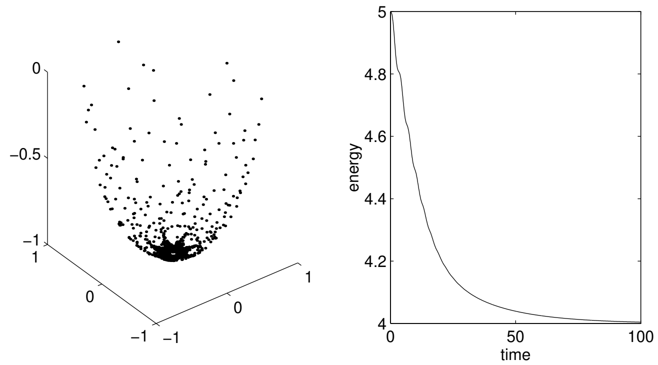

FIG. 6. (a) With normalization ($R \equiv 1$), the skinny top now converges to the "hanging down" configuration. (b) energy for the normalized Runge-Kutta method. Parameters and initial data are as in 3.

We now make the numerical problem slightly more difficult by considering a "skinny top" ($I_3 = 0.1$) with the same initial data and stepsize. Again, we first attempted to use the Runge-Kutta method. The periodic orbit was again correctly computed, with similar energy error as for the spherical top; however, the quasiperiodic trajectory is now completely wrong (Fig. 3a): the top spirals in toward the upright equilibrium position which has apparently become an asymptotically stable (i.e. dissipative) fixed point of the discrete map! Note that there is no such artificial behavior present in the symplectic solution (Fig. 4).

Since the variables u_i in the description of the top play a similar role to quaternions, it might be argued that the problem with the Runge-Kutta top simulation is that the length $R = \sqrt{u_1^2 + u_2^2 + u_3^2}$ of $\boldsymbol{u}$ is decaying with time (Fig 5). Would normalizing this vector at each timestep improve the results? This normalization does lead to a marked change in the simulation results, but not for the better! The top now gradually evolves towards the "hanging down" position (Fig. 6). In Fig. 6b, we also that the energy error is now substantially worse.

Similarly poor results were obtained when we rescaled the angular momenta $\boldsymbol{\pi}$ in order to preserve the energy at each step.

If we hold the time interval fixed and decrease the stepsize, we will of course eventually

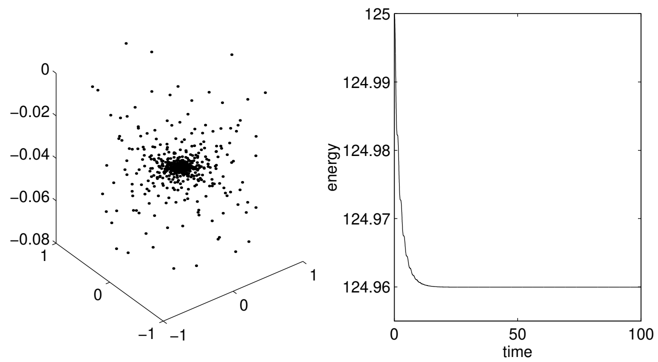

FIG. 7. The Runge-Kutta trajectory of the skinny top from $\boldsymbol{u} = (0, 1, 0)$, $\boldsymbol{\pi} = (0, 0, -5)$, $\Delta t = .02$.

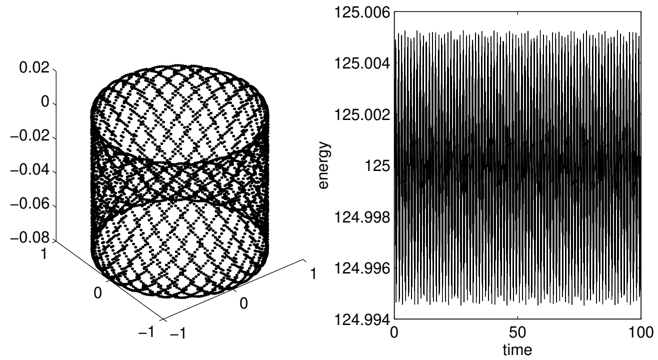

FIG. 8. The symplectic trajectory of the skinny top from $\boldsymbol{u} = (0, 1, 0)$, $\boldsymbol{\pi} = (0, 0, -5)$, $\Delta t = 0.02$.

obtain correct results from the Runge-Kutta method, but the appearance of such an artificial structure in an otherwise *apparently stable numerical computation* is very disturbing. Moreover, we note that the energy (Fig. 3c) is reasonably well preserved (to within 10%), so it would not be immediately obvious from examination of the energy that the results were entirely incorrect. To highlight this observation, we performed the same calculation, increasing $\boldsymbol{\pi}(0)$ by a factor of five and decreasing the stepsize by a corresponding factor. The resulting trajectory and energy error are shown in Fig. 7. Despite the totally incorrect dynamics, the energy is conserved to within 0.0004! The corresponding solution using the symplectic method is still well behaved and is, in fact, a good approximation to the correct dynamics (Fig. 8).

This example demonstrates some of the reasons why we are interested in symplectic methods. We have seen that a popular standard method can introduce artificial dynamical behavior in the simulation of simple rigid body problems, at timesteps for which a lower-order symplectic splitting method is well-behaved. In the next section, we will describe the extension of the splitting method which is needed for treating systems of rigid bodies.

III. THE SPLITTING METHOD FOR RIGID BODY SYSTEMS

We consider systems of (presumably a large number of) rigid bodies moving and rotating in three dimensions, with conservative forces acting on and between them. As in standard (e.g. quarternion) models, the orientation of each body is specified by the rotation which it has undergone from a fixed reference configuration. But now there are two new features: (i) we represent this rotation by a 3×3 matrix $\boldsymbol{Q}$; (ii) we add a constraint that this matrix actually be a rotation, namely $\boldsymbol{Q}^T\boldsymbol{Q} = \mathbf{1}$. Then the system may be conveniently described, and treated, using the methods of constrained Hamiltonian dynamics. These methods make it easy to derive not only the equations of motion for complex systems[12] but also good geometric integrators for them.[15,17,19,20]

We denote the total mass of the ith rigid body by m_i, the position of its center of mass by $\boldsymbol{q}_i$, linear momentum by $\boldsymbol{p}_i$, orientation by $\boldsymbol{Q}_i$, and angular momentum in the body frame, stored in a vector, by $\boldsymbol{\pi}_i$. Here $\boldsymbol{q}_i$, $\boldsymbol{p}_i$, and $\boldsymbol{\pi}_i$ are vectors in $\mathbf{R}^3$ and $\boldsymbol{Q}_i$ is a 3×3 orthogonal matrix.[20,19]

The Hamiltonian for the total system is the total energy, given by the sum of the translational kinetic energy of each body, $T_i^{\text{trans}}(\boldsymbol{p}_i)$, the rotational kinetic energy of each body, $T_i^{\text{rot}}(\boldsymbol{\pi}_i)$, and the potential energy $V(\boldsymbol{q}, \boldsymbol{Q})$, which we take to depend on the positions and orientations of the bodies only and not on their momenta. That is,

$$\begin{aligned} T(\boldsymbol{p}, \boldsymbol{\pi}) &= \sum_i \left(T_i^{\text{rot}}(\boldsymbol{\pi}_i) + T_i^{\text{trans}}(\boldsymbol{p}_i)\right) \\ H(\boldsymbol{p}, \boldsymbol{\pi}, \boldsymbol{q}, \boldsymbol{Q}) &= T(\boldsymbol{p}, \boldsymbol{\pi}) + V(\boldsymbol{q}, \boldsymbol{Q}), \end{aligned} \tag{1}$$

where $T_i^{\text{trans}}(\boldsymbol{p}_i) = \sum_i |\boldsymbol{p}_i|^2/2m_i$.

We would now like to employ a leapfrog-like splitting approach as in Sec. 2.1, but there are several subtleties. Firstly, the flow of the free rigid body, due to $T_i^{\text{rot}}(\boldsymbol{\pi}_i)$, is expensive to compute. However, it can be approximated efficiently using a splitting method due to McLachlan[14] and Reich[13]. To retain the nice properties of Verlet the approximation must be time-reversible and symplectic. This gives a splitting method which is symplectic overall, time reversible, preserves total linear and angular momentum, and uses only one force evaluation and one rotation of each rigid body per time step.

Another difficulty is that the constraints $\boldsymbol{Q}_i^T\boldsymbol{Q}_i = \mathbf{1}$ must be applied to the potential term. The equations of motion for this term are[15]:

$$\begin{aligned} \frac{d}{dt}\boldsymbol{q}_i &= 0 \\ \frac{d}{dt}\boldsymbol{p}_i &= -\frac{\partial V}{\partial \boldsymbol{q}_i} \\ \frac{d}{dt}\boldsymbol{Q}_i &= 0 \\ \frac{d}{dt}\boldsymbol{\pi}_i &= -\sum_j \operatorname{rot}\left(\boldsymbol{Q}_i^T \frac{\partial V}{\partial \boldsymbol{Q}_j}\right) \end{aligned} \tag{2}$$

where the (l, m) entry of the matrix $\partial V/\partial \boldsymbol{Q}_i$ is just the derivative with respect to the corresponding element of $\boldsymbol{Q}_i$:

$$(\partial V/\partial \boldsymbol{Q}_i)_{l,m} = \partial V/\partial Q_i^{lm},$$

and the notation rot refers to a mapping of 3×3 matrices to vectors constructed by first computing the skew symmetric part $(A - A^T)$, then associating this to a vector in $\mathbf{R}^3$:

$$\operatorname{rot}(\boldsymbol{A}) := \frac{1}{2}\operatorname{skew}^{-1}(\boldsymbol{A} - \boldsymbol{A}^T),$$

where

$$\operatorname{skew}(\boldsymbol{v}) := \begin{pmatrix} 0 & v^3 & -v^2 \\ -v^3 & 0 & v^1 \\ v^2 & -v^1 & 0 \end{pmatrix}. \tag{3}$$

Since $\boldsymbol{q}_i$ and $\boldsymbol{Q}_i$ are constant, these equations are easily solved.

The constrained differential equations due to the (translational and rotational) kinetic energies are

$$\begin{aligned} \frac{d}{dt}\boldsymbol{q}_i &= \boldsymbol{p}_i/m_i \\ \frac{d}{dt}\boldsymbol{p}_i &= 0 \\ \frac{d}{dt}\boldsymbol{Q}_i &= \boldsymbol{Q}_i \operatorname{skew}(\boldsymbol{I}_i^{-1}\boldsymbol{\pi}_i) \\ \frac{d}{dt}\boldsymbol{\pi}_i &= \boldsymbol{\pi}_i \times (\boldsymbol{I}_i^{-1}\boldsymbol{\pi}_i) \end{aligned} \tag{4}$$

where the 3×3 matrix $\boldsymbol{I}_i$ is the moment of inertia tensor of the ith rigid body.

The motion of the centers of mass is

$$\boldsymbol{q}_i(t) = \boldsymbol{q}_i(0) + \Delta t\ \boldsymbol{p}_i/m_i \tag{5}$$

and need not be considered further. (As the bodies are now uncoupled, we temporarily drop the subscript i.)

In practice, at this point we change variables to the principle axis of each body, so we can assume that $\boldsymbol{I}$ is diagonal. Now we note that the rotational part of (4) is a sum of three rigid bodies, with inertia tensors $\boldsymbol{I}^{(j)}$, $j = 1, 2, 3$, each with a single nonzero entry I_j on the diagonal. The motion of a rigid body with such a simple inertia tensor *can* be found in terms of elementary functions. For example, in x it is

$$\mathcal{G}_x(t): \quad \begin{cases} \boldsymbol{Q}(t) = \boldsymbol{Q}_0 \boldsymbol{R}_x(\theta)^{\mathrm{T}} \\ \boldsymbol{\pi}(t) = \boldsymbol{R}_x(\theta)\boldsymbol{\pi}_0 \end{cases} \tag{6}$$

where $\boldsymbol{R}_x(\theta)$ is a rotation about the x-axis by an angle $\theta = t\pi_1/I_1$. In practice, we use rational orthogonal approximations to the rotations (see the Appendix 1).

Notice that the constraint $\boldsymbol{Q}^T\boldsymbol{Q} = \mathbf{1}$, although used implicitly in the derivation, never needs to be artificially enforced. The matrices $\boldsymbol{Q}_i$ are always orthogonal because they are only ever changed by multiplication by an elementary orthogonal matrix.

The updates $\mathcal{G}_x$, $\mathcal{G}_y$, $\mathcal{G}_z$ constructed in this way are symplectic and preserve the total angular momentum of each body. We now compose them so as to approximate the flow of the whole body. That is, we apply them sequentially while retaining the important time-reversible property:

$$\mathcal{G}_x(\frac{1}{2}\Delta t)\mathcal{G}_y(\frac{1}{2}\Delta t)\mathcal{G}_z(\Delta t)\mathcal{G}_y(\frac{1}{2}\Delta t)\mathcal{G}_x(\frac{1}{2}\Delta t). \tag{7}$$

The above equations (5,6,7) now define the approximate motion due to the kinetic energy term $T(\boldsymbol{p}, \boldsymbol{\pi})$ in (1). Eqs. (2) define the exact motion due to the potential energy term $V(\boldsymbol{q}, \boldsymbol{Q})$. In a long simulation we merely apply these two updates alternately, thus using one force evaluation and one rigid body rotation per time step. There is some subtlety in ensuring that the overall order of the method is still two—see Appendix 2. An alternative to Eq. (7) that uses fewer rotations, and is much more accurate for nearly symmetric bodies, is discussed in Appendix 3.

IV. APPLICATION: TIP4P WATER

Due to the importance of water and aqueous solutions we perform a molecular dynamics simulation of water as a first benchmark for our integration scheme. In our model, rigid water monomers interact with a TIP4P intermolecular potential function.[23] The potential is based on the early ideas of Bernal and Fowler[24] and comprises three point charges together with an oxygen-oxygen Lennard-Jones term. The charges are located at the two hydrogen atoms and on the symmetry axes of the molecule. Details of our potential parameters can be found elsewhere.[23] TIP4P has been widely used in molecular dynamics and Monte Carlo calculations on liquid water, ice and hydrated proteins. However, it cannot be expected to reproduce the true potential accurately because its simple form ignores important non-additive polarization effects in water.

We compare our symplectic method with a quaternion/extrapolation scheme based on a Gragg-Bulirsch-Stoer (GBS) integrator with adaptive step size.[8] GBS is not symplectic but known for high-accuracy solutions to ordinary differential equations with low computational effort. The adaptive step size is not crucial for our results. Both methods have been implemented in the software package ORIENT[25] which can treat interacting molecules in a flexible and accurate way. Details of the implementation are given in Appendix 1.

We have seen in the top example (Sec. 3) that integrals of motion (total energy, overall angular and linear momentum, etc.) do not tell the whole story regarding physical realism. Nonetheless, to have any hope of dynamical fidelity these quantities must be approximately conserved in a molecular dynamics simulation. We measure absolute total energy values and the standard deviation $\sigma_{\rm rel}(E)$ of the total energy relative to its absolute mean value,

$$\sigma_{\rm rel}(E) = \frac{\sigma(E)}{\bar{E}} , \tag{8}$$

with

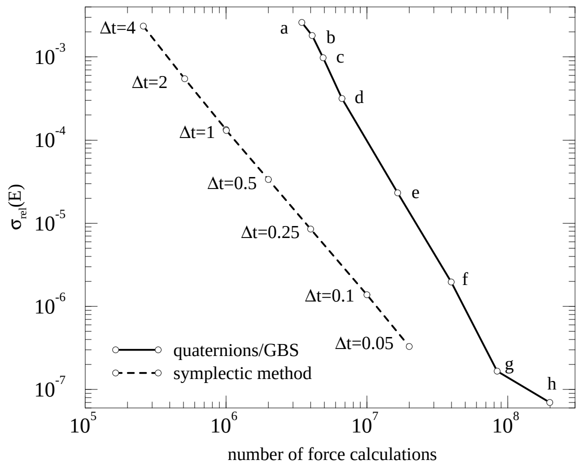

FIG. 9. Relative standard deviation of the trimer energy which results from a given number of force calculations for a 1 ns trajectory. The symplectic method requires far fewer force calculations for the same accuracy compared to quaternion/extrapolation with adaptive step size (simulations a-h).

$$\sigma(E) = \left[\frac{1}{N-1}\left(\left(\sum_{j=1}^{N} E_j^2\right) - N\bar{E}^2\right)\right]^{\frac{1}{2}}$$

$$\bar{E} = \frac{1}{N}\sum_{j=1}^{N} E_j \ .$$

E_j denotes the energy value at the j-th evalution, and all relevant variables are evaluated every 100 fs. This should be long enough to avoid correlation effects.

In order to measure the computational costs we calculate also the number of force evaluations needed for a certain accuracy. This number is the crucial parameter for efficiency of an integration scheme because the calculation of forces typically dominates the costs. It should be easy to convert this number into real computational time for any given implementation of the force calculation on a particular computer.

In our first example we solve Newton's equations of motion for trajectories of 1 ns for a water trimer $(H_2O)_3$ at fixed total energy (50 kJ/mol). At this energy the water cluster is stable and we observe only a few isomerizations. All trajectories start from the cyclic global minimum with no overall angular and linear momentum.

At the beginning we focus on the computational costs and plot the standard deviation of the total energy $\sigma_{\rm rel}(E)$ versus the number of force calculations in Fig. 9. The figure shows how the new method outperforms quaternion/extrapolation in efficiency. A quaternion/GBS simulation needs up to ten times more force calculations in order to achieve the same accuracy. For example, the new symplectic method needs about 1 million force evaluations for a $\sigma_{\rm rel}(E) = 10^{-4}$ whereas quaternion/GBS requires 10 million evaluations for the same accuracy in this simulation.

Another important difference becomes clear if we look at the evolution of the total energy as a function of integration time (Fig. 10 and 11). Quaternion/extrapolation produces a

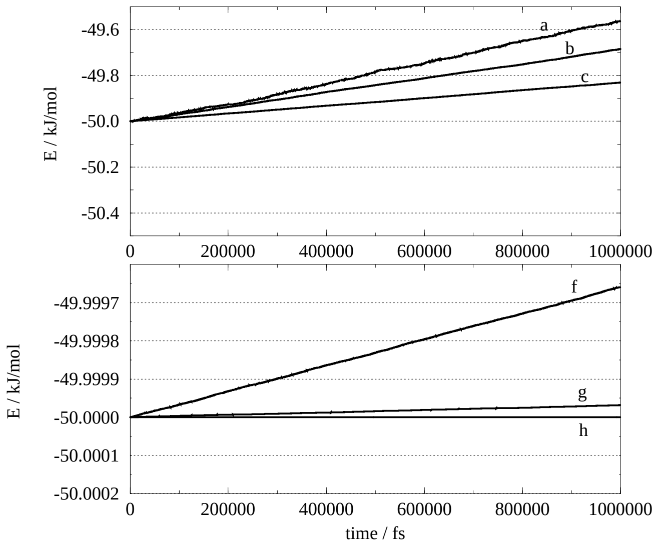

FIG. 10. Evolution of total energy for the three lowest (top) and highest (bottom) accuracies in Fig. 9 for a quaternion/extrapolation integration scheme. All curves are smooth but drift away from the initial energy.

smooth but growing total energy. Higher accuracy can reduce the effect but cannot eliminate the underlying drift. This can also be seen in the evolution of the standard deviation $\sigma_{\mathrm{rel}}(E)$ in Fig. 12. In contrast, if we look at the same plot for the symplectic method we see an oscillating but stable evolution of the total energy even at low accuracy (Fig. 11). Stability in our example is lost only for time steps which lead to accuracies below the lowest one shown in Fig. 9 ($\Delta t > 4\,\mathrm{fs}$).

We now turn to the modulus of the overall linear and angular momenta (Fig. 13 and 14),

$$\begin{aligned} P_{\mathrm{lin}} &= \left| \sum_{i=1}^{N} \boldsymbol{p}_i \right| \\ P_{\mathrm{ang}} &= \left| \sum_{i=1}^{N} \boldsymbol{r}_i \times \boldsymbol{p}_i + \boldsymbol{\pi'}_i \right| , \end{aligned} \tag{9}$$

where N is the number of molecules, $\boldsymbol{r}_i$ denotes the vector between the centre of mass of molecule i and the centre of mass of the whole system, $\boldsymbol{p}_i$ is the linear momentum of molecule i and $\boldsymbol{\pi'}_i$ the corresponding angular momentum in the same coordinate system.

The overall linear momentum is in principle conserved by both methods. Therefore, it can serve to assess numerical rounding errors due to machine accuracy. These errors should increase with higher numbers of force evaluations. Fig. 13 illustrates this effect.

However, in contrast to our symplectic method quaternion/extrapolation does not conserve the overall angular momentum in principle. The resulting difference becomes obvious in Fig. 14. For quaternion/GBS the initially vanishing overall rotation is decreasing with increasing accuracy. Nonetheless, it remains several orders of magnitude higher than for the symplectic method. The latter only suffers from accumulation of rounding error which grows with the number of force calculations. However, overall rotation remains negligible for the symplectic method.

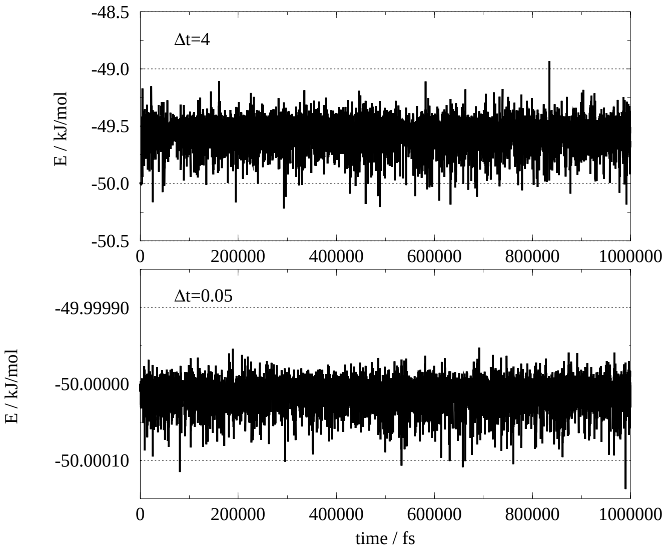

FIG. 11. The figure shows the total energy for the biggest (top) and the smallest (bottom) step size used in Fig. 9 with the symplectic integration scheme. We always observed stable oscillation around the starting energy of 50 kJ/mol. The initial shift to higher energy in the top graph in an entropic effect due to starting at the global minimum and disappears for less distinguished starting points.

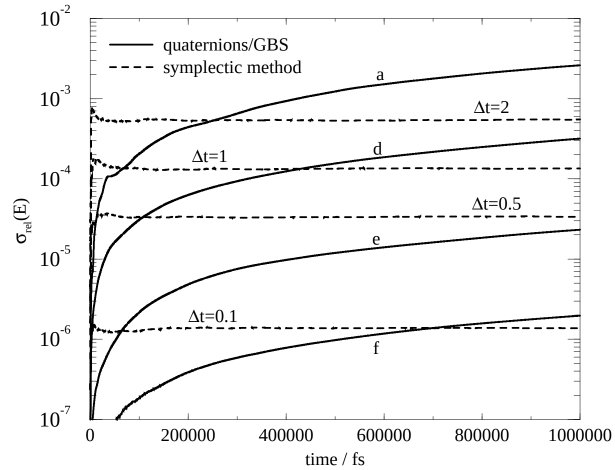

FIG. 12. The plot of representative standard deviations shows again the drift in energy for quaternion/extrapolation trajectories, whereas the symplectic methods leads to stable energy conservation.

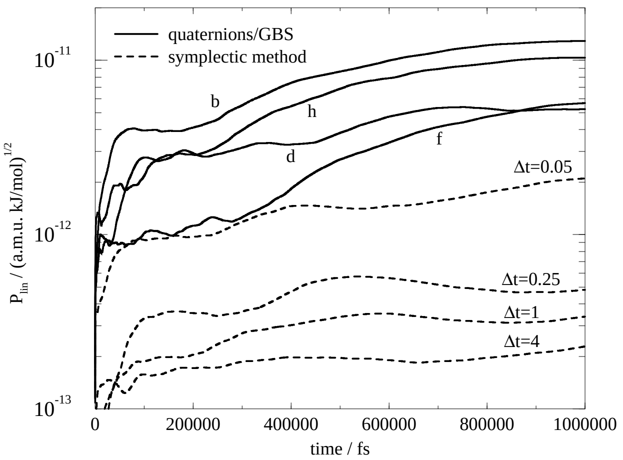

FIG. 13. The initially vanishing overall linear momentum is in principle conserved by both methods. Therefore, the above plot gives an estimate of numerical rounding errors due to machine accuracy.

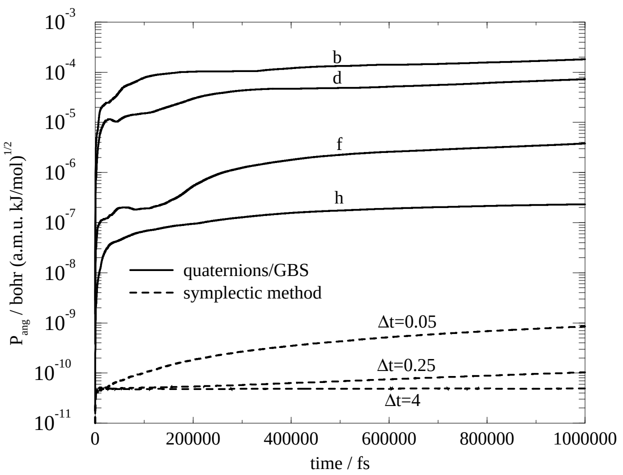

FIG. 14. Evolution of the overall angular momentum during the integration. The symplectic methods conserves the initially vanishing angular momentum much more accurately. Notice that smaller step sizes in this method lead to slightly more overall rotation of the system.

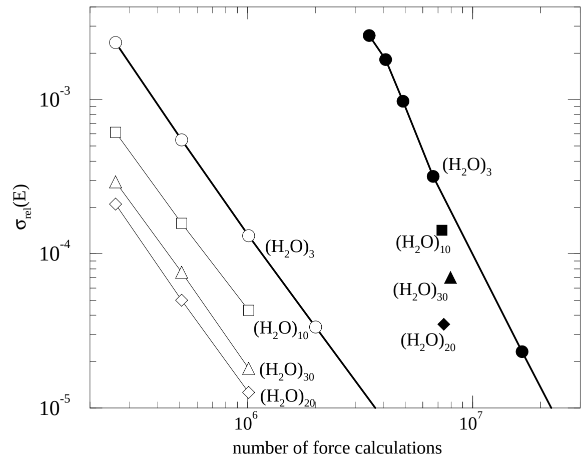

FIG. 15. Computational efficiency of both methods for different model systems. For bigger systems the symplectic method (opaque symbols) performs increasingly better than the quaternion/extrapolation scheme (filled symbols). Results for $(H_2O)_{10}$, $(H_2O)_{20}$ and $(H_2O)_{30}$ comprise symplectic simulations with $\Delta t = 1, 2, 4\,\mathrm{fs}$ (i.e. 1000000, 500000 and 250000 force calculations) and one representative quaternion/Gragg-Bulirsch-Stoer run (compare Fig. 9).

We did not observe nonphysical effects in any of the simulations. Both methods produced consistent results compared with a systematically different method: Monte Carlo sampling and normal mode analysis. We compared ensemble averages like caloric curves from microcanonical molecular dynamics simulations with transformed Monte Carlo results for the canonical ensemble. We also reproduced intermolecular normal mode frequencies with dipole autocorrelation functions in low energy molecular dynamics runs.

Finally we demonstrate that this comparison holds also for bigger systems. We did some simulations for $(H_2O)_{10}$, $(H_2O)_{20}$ and $(H_2O)_{30}$ with the same intermolecular potential and obtained very similar results. Fig. 15 shows the performance for three different time steps ($\Delta t = 1, 2, 4\,\mathrm{fs}$) in the symplectic integration and one representative quaternion/GBS result for each of the model clusters. It suggests that the gap between the new method and non-symplectic quaternion/extrapolation increases with system size. Simulations at different total energies did not show any significant differences and underlined the above conclusions.

V. SUMMARY

We have presented a powerful method for rigid body molecular simulations of the type commonly used in chemical and physical studies. The symplectic splitting method is stable, and more reliable than standard quaternion integration methods, since it mimics physical properties of the true flow of the continuous time problem. Moreover, the integrator is efficiently implemented in terms of a few planar rotations per rigid body at each timestep, and is comparable in terms of work per timestep to the standard quaternionic integrator. Numerical calculations demonstrate the superiority of the symplectic method to the standard approach.

While the new method is in some respects comparable to SHAKE-based symplectic rigid body schemes,[7,10] those methods sacrifice something in terms of robustness (since they require the solution of a nonlinear system using some iterative solver) and in terms of computational complexity. However, the SHAKE-based methods readily generalize to systems of rigid bodies *connected by constraints*[10] (e.g. joints or rods), whereas the splitting method discussed here does not.

ACKNOWLEDGMENTS

We are grateful to Dr. David Wales for several discussions. B.L. is supported by the National Science Foundation, grant number NSF-9303223. A.D. is a Marie Curie Fellow of the European Union and a scholar of the Studienstiftung des Deutschen Volkes.

APPENDIX 1. IMPLEMENTATION

This appendix is intended to demonstrate how easily the symplectic method can be implemented in a molecular dynamics program.

A molecule can be described by a centre of mass position vector $\boldsymbol{q}$, a orientation matrix $\boldsymbol{Q}$ and vectors for its linear and angular momentum ($\boldsymbol{p}$ and $\boldsymbol{\pi}$). The elements of $\boldsymbol{Q}$ are the direction cosines between the global axes system and a local molecule-fixed frame. Positions $\boldsymbol{q}$ and momenta $\boldsymbol{p}$ of the translational degrees of freedom will be propagated in a simple leapfrog scheme. It will maintain the symplecticity of the integration.

In the first step we need to calculate linear force vectors $\boldsymbol{f}^n$ and torques $\boldsymbol{\tau}^n$ at time $t_n \equiv t_0 + n\Delta t$ for all molecules in the system. Both are functions of all position vectors $\boldsymbol{q}$ and rotation matrices $\boldsymbol{Q}$.

Having calculated the forces we can start the integration itself and propagate the momenta of all molecules from time t_n to t_{n+1}:

$$\begin{aligned} \boldsymbol{\pi}^{n+\frac{1}{2}} &= \boldsymbol{\pi}^n + \frac{1}{2}\Delta t\ \boldsymbol{\tau}^n \\ \boldsymbol{p}^{n+\frac{1}{2}} &= \boldsymbol{p}^n + \frac{1}{2}\Delta t\ \boldsymbol{f}^n\ . \end{aligned} \tag{10}$$

Then we move the centre of mass position a full time step,

$$\boldsymbol{q}^{n+1} = \boldsymbol{q}^n + \Delta t\ \boldsymbol{p}^{n+\frac{1}{2}}\ .$$

We now apply consecutive rotations $\boldsymbol{R}_1$ to $\boldsymbol{R}_5$ to all angular momenta and update all orientation matricies for a full time step from t_n to t_{n+1},

$$\begin{aligned} \boldsymbol{R}_1 &:= \boldsymbol{R}_{\mathrm{x}}(\frac{1}{2}\Delta t\frac{\pi_1}{I_1});\ \boldsymbol{\pi} = \boldsymbol{\pi}\ \boldsymbol{R}_1;\ \boldsymbol{Q} = \boldsymbol{Q}\ \boldsymbol{R}_1^{\mathrm{T}} \\ \boldsymbol{R}_2 &:= \boldsymbol{R}_{\mathrm{y}}(\frac{1}{2}\Delta t\frac{\pi_2}{I_2});\ \boldsymbol{\pi} = \boldsymbol{\pi}\ \boldsymbol{R}_2;\ \boldsymbol{Q} = \boldsymbol{Q}\ \boldsymbol{R}_2^{\mathrm{T}} \\ \boldsymbol{R}_3 &:= \boldsymbol{R}_{\mathrm{z}}(\ \Delta t\frac{\pi_3}{I_3});\ \boldsymbol{\pi} = \boldsymbol{\pi}\ \boldsymbol{R}_3;\ \boldsymbol{Q} = \boldsymbol{Q}\ \boldsymbol{R}_3^{\mathrm{T}} \end{aligned}$$

$$\boldsymbol{R}_4 := \boldsymbol{R}_{\rm y}(\frac{1}{2}\Delta t\frac{\pi_2}{I_2});\ \boldsymbol{\pi} = \boldsymbol{\pi}\ \boldsymbol{R}_4;\ \boldsymbol{Q} = \boldsymbol{Q}\ \boldsymbol{R}_4^{\rm T}$$
$$\boldsymbol{R}_5 := \boldsymbol{R}_{\rm x}(\frac{1}{2}\Delta t\frac{\pi_1}{I_1});\ \boldsymbol{\pi} = \boldsymbol{\pi}\ \boldsymbol{R}_5;\ \boldsymbol{Q} = \boldsymbol{Q}\ \boldsymbol{R}_5^{\rm T}\ ,$$

where I_1, I_2, I_3 are elements of the diagonal inertia tensor of a molecule and π_1, π_2, π_3 are the corresponding components of $\boldsymbol{\pi}$ in the principal axes system. $\boldsymbol{R}_{\rm x}(\phi)$ denotes a rotation around the x-axis by an angle ϕ and $\boldsymbol{R}_i^{\rm T}$ is the transpose of $\boldsymbol{R}_i$. A computationally efficient representation of $\boldsymbol{R}_{\rm x}(\phi)$ is for example

$$\boldsymbol{R}_{\rm x}(\phi) = \begin{pmatrix} 1 & 0 & 0 \\ 0 & \frac{1-\phi^2/4}{1+\phi^2/4} & -\frac{\phi}{1+\phi^2/4} \\ 0 & \frac{\phi}{1+\phi^2/4} & \frac{1-\phi^2/4}{1+\phi^2/4} \end{pmatrix}\ ,$$

and all other rotations follow straightforwardly.

After obtaining $\boldsymbol{q}^{n+1}$ and $\boldsymbol{Q}^{n+1}$ for all molecules we can now calculate the forces $\boldsymbol{f}^{n+1}$ and torques $\boldsymbol{\tau}^{n+1}$ and propagate the momenta another half time step:

$$\boldsymbol{p}^{n+1} = \boldsymbol{p}^{n+\frac{1}{2}} + \frac{1}{2}\Delta t\ \boldsymbol{f}^{n+1}$$
$$\boldsymbol{\pi}^{n+1} = \boldsymbol{\pi}^{n+\frac{1}{2}} + \frac{1}{2}\Delta t\ \boldsymbol{\tau}^{n+1}\ .$$

This is the end of one integration step. Since the forces and torques are not dependent on the momenta we do not need to calculate the forces again but can start directly with the first half time step for the momenta (Eq. 10).

The method is implemented in our package ORIENT[25] which also incorporates the quaternion/GBS algorithm with adaptive stepsize[8] as an alternative. ORIENT is a program for carrying out calculations of various kinds for an assembly of interacting molecules. It uses a site-site potential specified by the user, including electrostatic, induction, repulsion, dispersion and charge-transfer interactions if required.[27] The electrostatic interactions may be described by simple point charges or by more elaborate descriptions involving distributed multipoles.[27] Distributed polarizabilities may be used if required, and the site-site repulsion and dispersion and charge-transfer terms may be anisotropic. In the above calculations we did not use any potential cut-off or other changes to the intermolecular TIP4P potential.[23]

A. Computation of Interbody Forces

In the formulation of the equations motion, we need to compute the derivatives of the potential with respect to center of mass and rotational components. In this section we show that this procedure is straightforward for both site-to-site and dipolar interactions.

1. Site-Site Potentials

In our application (Sec. 5), we suppose each rigid body is composed of a number of point masses that interact pairwise with the point masses in the other rigid bodies. They do not interact within one body, because their relative positions are held fixed. Suppose the (symmetric) pair potential of two point masses located at $\boldsymbol{x}$ and $\boldsymbol{y}$ is $W(\boldsymbol{x},\boldsymbol{y})$, creating a force $\boldsymbol{f} = -\nabla_{\boldsymbol{x}} W(\boldsymbol{x},\boldsymbol{y})$ on the mass at $\boldsymbol{x}$. To keep the equations clear we will write them out for the case of a single particle mounted on each body, at $\boldsymbol{x}_i$ in the reference configuration for body i. After time t it has reached the location $\boldsymbol{\xi}_i(t) := \boldsymbol{Q}_i(t)\boldsymbol{x}_i + \boldsymbol{q}_i(t)$. The total potential energy is then

$$V(\boldsymbol{q},\boldsymbol{Q}) = \sum_{j>i} W(\boldsymbol{Q}_i(t)\boldsymbol{x}_i + \boldsymbol{q}_i(t), \boldsymbol{Q}_j(t)x_j + \boldsymbol{q}_j(t)) \tag{11}$$

giving derivatives

$$\begin{aligned} \frac{\partial V}{\boldsymbol{q}_i} &= -\sum_{j>i} \boldsymbol{f}(\boldsymbol{\xi}_i,\boldsymbol{\xi}_j) \\ \frac{\partial V}{\boldsymbol{Q}_i} &= -\sum_{j>i} \boldsymbol{f}(\boldsymbol{\xi}_i,\boldsymbol{\xi}_j)\boldsymbol{x}_i^T \end{aligned} \tag{12}$$

and the differential equations (2) due to the potential are

$$\begin{aligned} \frac{d}{dt}\boldsymbol{q}_i &= 0 \\ \frac{d}{dt}\boldsymbol{p}_i &= \sum_{j>i} \boldsymbol{f}(\boldsymbol{\xi}_i,\boldsymbol{\xi}_j) \\ \frac{d}{dt}\boldsymbol{Q}_i &= 0 \\ \frac{d}{dt}\boldsymbol{\pi}_i &= \sum_{j>i} \operatorname{rot}(\boldsymbol{Q}_i^T \boldsymbol{f}(\boldsymbol{\xi}_i,\boldsymbol{\xi}_j)\boldsymbol{x}_i^T) \\ &= \sum_{j>i} (\boldsymbol{Q}_i^T \boldsymbol{f}(\boldsymbol{\xi}_i,\boldsymbol{\xi}_j)) \times \boldsymbol{x}_i \end{aligned} \tag{13}$$

We use these equations together with $\boldsymbol{f}(\boldsymbol{\xi}_i,\boldsymbol{\xi}_j)$ supplied by standard ORIENT routines for the interparticle forces.

2. Dipolar Soft Spheres

Dipolar soft sphere models can also be handled. We suppose an interbody potential between particles i and j of the form[7,21,22]

$$V = V(\boldsymbol{q}_i,\boldsymbol{Q}_i,\boldsymbol{q}_j,\boldsymbol{Q}_j) = V_{\text{s.r.}} + V_{\text{d}},$$

where $V_{\text{s.r.}}$ consists of short range interactions and V_{d} represents the dipole-dipole terms:

$$V_{\text{s.r.}} = 4\epsilon \left(\frac{\sigma}{r_{ij}}\right)^{12},$$

$$V_{\mathrm{d}} = \frac{1}{r_{ij}^3}\boldsymbol{\mu}_i \cdot \boldsymbol{\mu}_j - \frac{3}{r_{ij}^5}(\boldsymbol{\mu}_i \cdot \boldsymbol{r}_{ij})(\boldsymbol{\mu}_j \cdot \boldsymbol{r}_{ij}),$$

where

$$\boldsymbol{r}_{ij} = \boldsymbol{q}_i - \boldsymbol{q}_j, \qquad\qquad r_{ij} = \|\boldsymbol{r}_{ij}\|,$$

and $\boldsymbol{\mu}_i$ denotes the orientation of the ith dipole vector, easily expressed in terms of the rotation matrix $\boldsymbol{Q}_i$ and some initial fixed reference orientation $\bar{\boldsymbol{\mu}}_i$:

$$\boldsymbol{\mu}_i(t) = \boldsymbol{Q}_i \bar{\boldsymbol{\mu}}_{\boldsymbol{i}}.$$

Evaluation of the derivatives of the various terms with respect to the center of mass positions ($\boldsymbol{q}_i$) is straightforward. The derivatives of the dipolar potential with respect to the components of the rotation matrix are also straightforward if we express V_{d} in terms of the individual components of $\boldsymbol{Q}_i$, $\bar{\boldsymbol{\mu}}_{\boldsymbol{i}}$:

$$\boldsymbol{Q}_i = (Q_i^{kl}), 1 \leq k, l \leq 3, \qquad\qquad \bar{\boldsymbol{\mu}}_i = (\bar{\mu}_i^1, \bar{\mu}_i^2, \bar{\mu}_i^3).$$

For example,

$$\boldsymbol{\mu}_i \cdot \boldsymbol{\mu}_{\boldsymbol{j}} = \sum_k \sum_l \sum_m Q_i^{lk} Q_j^{lm} \mu_i^k \mu_j^m$$

with derivatives

$$\frac{\partial}{\partial Q_i^{lk}}(\boldsymbol{\mu}_i \cdot \boldsymbol{\mu}_{\boldsymbol{j}}) = \sum_m Q_j^{lm} \mu_i^k \mu_j^m,$$

Similar expressions hold for the other terms and allow us to work out the full derivatives. This approach can be extended to treat other multipole approximations[27] as well.

APPENDIX 2. SECOND ORDER ACCURACY OF THE SPLITTING METHOD

If we denote the time-Δt solution of Hamiltonian H by $\exp_H(\Delta t)$, then the Verlet or leapfrog method of Sec. 2.1 can be written

$$\exp_T(\frac{1}{2}\Delta t)\exp_V(\Delta t)\exp_T(\frac{1}{2}\Delta t).$$

When we take a large number, n of time steps in a row, the total update can be written

$$\exp_T(\frac{1}{2}\Delta t)(\exp_V(\Delta t)\exp_T(\Delta t))^n \exp_T(-\frac{1}{2}\Delta t),$$

because of the "flow property" $\exp_T(a)\exp_T(b) = \exp_T(a+b)$. Essentially one need only alternate the updates due to V and T.

In the rigid body splitting method, we do not use the exact solution $\exp_T$, but an approximation to it, say ϕ_T. This approximation will not have the flow property. However, for the method

$$\exp_V(\frac{1}{2}\Delta t)\phi_T(\Delta t)\exp_V(\frac{1}{2}\Delta t) \quad (14)$$

n steps take the form

$$\exp_V(\frac{1}{2}\Delta t)(\phi_T(\Delta t)\exp_V(\Delta t))^n \exp_V(-\frac{1}{2}\Delta t)$$

so that we can still alternate the two updates, as before. (If *both* pieces of the Hamiltonian had been approximated, this result would no longer hold.) The basic method (14) is second order because it has the time-symmetry property $f(\Delta t)f(-\Delta t) = 1$.[3]

APPENDIX 3. SPECIAL RIGID BODY UPDATES

Although the solution of the rigid body system with Hamiltonian $T(\boldsymbol{\pi}, \boldsymbol{Q}) = \sum_{i=1}^{3} \pi_i^2/2I_i$ and constraint $\boldsymbol{Q}^T\boldsymbol{Q} = \mathbf{1}$ in general involves elliptic functions,[26] there is one common special case which does not. This is the symmetric rigid body with (say) $I_1 = I_2$ (in principal coordinates), e.g. NH_3. Then it is well known that (i) the momentum evolves by a planar rotation, and (ii) the orientation evolves by a combination of this rotation and a secondary rotation about the axis defined by the angular momentum. The solution in this case is

$$\begin{aligned} \boldsymbol{\pi}(t) &= \boldsymbol{R}_z\boldsymbol{\pi}_0 \\ \boldsymbol{Q}(t) &= \boldsymbol{Q}_0\boldsymbol{R}_z^T\boldsymbol{R}_{\boldsymbol{\pi}_0}^T \end{aligned} \quad (15)$$

where $\boldsymbol{R}_z$ is rotation about the z-axis by angle $t(1/I_3 - 1/I_2)$, and $\boldsymbol{R}_{\boldsymbol{\pi}_0}$ is rotation about angle $\boldsymbol{\pi}_0$ by angle $t|\boldsymbol{\pi}_0|/I_2$. This rotation can be expressed in terms of the matrix exponential as $e^{t\,\mathrm{skew}(\boldsymbol{\pi}_0)}$ or evaluated in terms of trigonometric functions.

If the body is truly symmetric then it may not be necessary to remember its rotation about its axis of symmetry, and the factor $\boldsymbol{R}_z^T$ in the $\boldsymbol{Q}$ update (Eq. (15)) can be omitted.

This update not only replaces the five rotations needed in Eq. (7) by one (slightly more complicated) rotation, it is also exact. Thus in situations where error committed by Eq. (7) might be large, i.e., when a relatively large proportion of the total energy of the system is in the rotational kinetic energy of the bodies, this update will lead to a much more accurate update overall.

In one test with two rigid bodies and initially half the energy as rotational kinetic energy, this method was found to be twice as fast in the rigid body updates and ten times as accurate overall.

Furthermore we can apply this idea to *general* rigid bodies as well. We partition the Hamiltonian as

$$2T = \left(\frac{\pi_1^2}{I_2} + \frac{\pi_2^2}{I_2} + \frac{\pi_3^2}{I_3}\right) + \pi_1^2\left(\frac{1}{I_1} - \frac{1}{I_2}\right).$$

The first term corresponds to a symmetric rigid body, and the second evolves by a planar rotation as in Eq. (6). We can compose these into an overall rigid body update using three rotations, instead of the five in Eq. (7). Because the symmetric update is more complicated, we found no change in speed over Eq. (7), but for nearly symmetric bodies ($I_1 \approx I_2$), there were substantial improvements in accuracy.

Unfortunately, water is not symmetric enough! Its moments of inertia are proportional to 2.88, 1.88, and 1.00, and in practice we found only modest improvements using this modified scheme in the present application.

REFERENCES

[1] M.P. Allen, M.A. Warren, M.R. Wilson, A. Sauron and W. Smith, J. Chem. Phys. **105**, 2850 (1996); I. G. Tironi, R. M. Brunne and W. F. Van Gunsteren, Chem. Phys. Lett. **250**, 19 (1996)

[2] D.M.F. Van Aalten, A. Amadei, A.B.M. Linssen, V.G.H. Eijsink, G. Vriend, H.J.C. Berendsen, Proteins-structure function and genetics **22** (1), 45 (1995); C.S. Verma, L.S.D. Caves, R.E. Hubbard and G.C.K. Roberts, J. Mol. Bio. **266**, 776 (1997)

[3] M.P. Calvo and J.M. Sanz-Serna, *Numerical Hamiltonian Problems*, Chapman & Hall, London (1994).

[4] J. Wisdom and M. Holman, Astron. J. **102**, 1528 (1991).

[5] B. Leimkuhler, S. Reich and R.D. Skeel, *IMA Volumes in Mathematics and its Applications* **82**, p. 161, Spinger Verlag (1996).

[6] J. Frank, W. Huang and B. Leimkuhler, J. Comp. Phys. **133**, 160 (1997).

[7] A. Kol, B. Laird and B. Leimkuhler, J. Chem. Phys., to appear.

[8] W.H. Press, S.A. Teukolsky, W.T. Vettering and B.P. Flannery, *Numerical Recipes*, Cambridge University Press, Cambridge (1992).

[9] M.P. Allen and D.J. Tildesley, *Computer Simulation of Liquids*, Oxford Science, Oxford (1987).

[10] E. Barth and B. Leimkuhler, Fields Institute Communications **10**, 25 (1996).

[11] J.P. Ryckaert, G. Ciccotti and H.J.C. Berendsen, J. Comp. Phys. **23**, 327 (1977).

[12] J. Marsden and T. Ratiu, *An Introduction to Mechanics and Symmetry*, Springer-Verlag (1994).

[13] S. Reich, Physica D **76**, 375 (1994).

[14] R.I. McLachlan, Phys. Rev. Lett. **71**, 3043 (1993).

[15] S. Reich, Fields Institute Communications **10**, 181 (1996).

[16] R. Ruth, IEEE Trans. Nuc. Sci. **30**, 2669 (1983).

[17] B.J. Leimkuhler and R.D. Skeel, J. Comp. Phys. **112**, 117 (1994).

[18] G. Benettin and A. Giorgilli, J. Stat. Phys. **74**, 1117 (1994).

[19] S. Reich, SIAM J. Numer. Anal. **33**, 475 (1996).

[20] R.I. McLachlan and C. Scovel, J. Nonlinear Sci. **5** , 233 (1995).

[21] P.G. Kusalik, J. Chem. Phys. **93**, 3520 (1990).

[22] D. Wei and G.N. Patey, Phys. Rev. A **46**, 2043 (1992).

[23] W.L. Jorgensen, J. Chandrasekhar and J. Madura, J. Chem. Phys. **79**, 926 (1983).

[24] J.D. Bernal and R.H. Fowler, J. Chem. Phys. **1**, 515 (1933).

[25] A.J. Stone, A. Dullweber, M.P. Hodges, P.L.A. Popelier and D.J. Wales, ORIENT: *A program for studying interactions between molecules* Version 3.2, University of Cambridge (1995-97), *available at:* http://fandango.ch.cam.ac.uk.

[26] J.L. Synge and B.A. Griffith, *Principles of Mechanics*, McGraw-Hill, 1959.

[27] A.J. Stone, *The Theory of Intermolecular Forces*, Oxford University Press, Oxford (1996).